MECSOL 2024 - Proceedings of the 9th International Symposium on Solid Mechanics
P.T.R.de Mendonça, E.A.Fancello and C.R.M.Roesler (Editors), Florianópolis SC, Brazil, October 21st to 23th, 2024

Mechanical Energy Multi-Harvesting: On the Performance Enhancement of Mechanical Energy Harvesters

Luã Guedes Costa, Marcelo Amorim Savi

Universidade Federal do Rio de Janeiro, COPPE - Mechanical Engineering, Center for Nonlinear Mechanics, 21941-914 - Rio de Janeiro - RJ - Brazil

Abstract. Mechanical energy is manifested in the environment in various forms such as vibration, wind, sea waves, biomechanical motion, and sound. In this regard, the usage of different transducer mechanisms, especially smart materials, combined with mechanical nonlinear phenomena, has been extensively employed to convert mechanical into electrical energy, harnessing this kind of energy. Although many solutions are proposed, several challenges still exist in terms of implementation and performance. In this work, two recently proposed solutions for these challenges are summarized: the compactness of energy harvester to be implemented in confined spaces; and the ability to capture energy from multidirectional sources. These two solutions are distinguished by their multimodal characteristics associated with multi-transduction mechanisms. Results indicate that these features significantly enhance their energy harvesting capabilities, including maximum output power and bandwidth, outperforming classical counterparts.

Keywords: Energy Harvesting, Multi-Transduction, Nonlinear Systems, Multi-Degrees-of-Freedom, Smart Systems

INTRODUCTION

The advancement of semiconductor technology has significantly reduced the energy required to power various electronic devices, particularly IoT devices, standalone sensors, and micro-electromechanical systems (MEMS). Consequently, harvesting energy from mechanical sources has become an attractive option, as it provides sufficient power for these innovative devices (duToit et al., 2005).

Various transduction mechanisms are employed to convert mechanical energy from the environment into useful electrical energy. The most noteworthy mechanisms include electromagnetic transducers, triboelectric phenomena, and smart materials such as piezoelectric and magnetostrictive materials. Electromagnetic transducers operate based on the principle of electromagnetic induction, where a change in a magnetic field near a conductor induces a proportional electrical current (Faraday, 1832). Triboelectric transducers utilize the triboelectric effect, where electric charges accumulate due to contact and friction between two different materials, involving both contact electrification and electrostatic induction caused by the potential difference between the materials (Liu et al., 2021). Piezoelectric energy harvesting relies on the direct piezoelectric effect, which describes the electromechanical relationship between mechanical deformation and electrical voltage. When a piezoelectric material is deformed, it generates a proportional electrical voltage (IEEE, 1987). Magnetostrictive energy harvesting is based on the Villari effect (or inverse magnetostrictive effect). When stress is applied to a magnetostrictive material in the presence of a magnetic field, its magnetization changes. This effect can be combined with electromagnetic induction to harness mechanical energy (Apicella et al., 2019).

The deployment of these transducers typically involves integrating them into a primary structure, where the transducer is strategically positioned and attached to this structure. The most common energy harvesting design is based on the resonating cantilever beam structure, extensively documented in the literature. Its primary drawback lies in diminished performance when operating beyond the narrow resonance range (Erturk and Inman, 2009).

The inclusion of nonlinear modulations is one strategy to increase the performance of the cantilever-based devices. Many types of modulations were proposed. Multistable systems, either induced by magnetic interactions or compressive forces inducing buckling, are the most common nonlinear modulation reported in the literature. This modification has been shown to have the potential to enhance both bandwidth and maximum power harvested (Costa et al., 2021). Additionally, nonsmooth systems have been demonstrated to increase the bandwidth of operation of cantilever-based harvesters, at the cost of maximum power output (Ai et al., 2019). Moreover, structures leveraging the use of attached pendula, shape memory materials, rotational characteristics, asymmetry, and fluid-structure interactions are also reported to increase the

performance of conventional devices (Zou et al., 2019).

Another strategy to increase the performance of the conventional cantilever-based energy harvester is the inclusion of additional relevant degrees of freedom in the construction of the device. This approach increases the number of regions of operations, as it creates new regions of high performance due to resonance (Wu et al., 2013).

In this work, a new strategy to enhance performance, named multi-harvesting, is presented. Multi-harvesting allies the strategic positioning of new transducers with multimodal characteristics (new relevant degrees of freedom) as a means of enhancing performance. For that, two devices are presented: the compact multistable energy harvester (CMEH) as proposed in (Costa and Savi, 2024a; Costa et al., 2024), and the multidirectional hybrid energy harvester (MHEH) as proposed in (Costa and Savi, 2024b). These two harvesters are derived from the classical cantilever design, being modified based on the directives of the proposed multi-harvesting strategy. Results indicate that the incorporation of the new strategy increases the performance of both harvesters when compared to their classical counterparts.

HARVESTER DESIGNS AND PHYSICAL MODELING

In this section, both harvesters are briefly presented, and their mathematical models are showcased. These models are dimensionless mathematical systems of equations that capture the main qualitative characteristics of the harvesters, allowing a general overview of the physical characteristics and performance of both devices.

The Compact Multistable Energy Harvester

The conventional bistable energy harvester (CBEH) is composed of a cantilever beam working as a structural component. A piezoelectric patch is attached to the region near the beam's fixed end. A tip mass with a magnet is attached at the beam's free end. This magnet interacts with a fixed external magnet, and this interaction produces bistability. The compact multistable energy harvester (CMEH) is a natural evolution of the bistable energy harvester as displayed in Fig. 1. In the CMEH, the main beam is modified to accommodate an inner beam with identical characteristics, resulting in a space-efficient design. This design places two transducers in previously unused space and introduces additional magnetic interactions, producing a compact harvester with multistable characteristics.

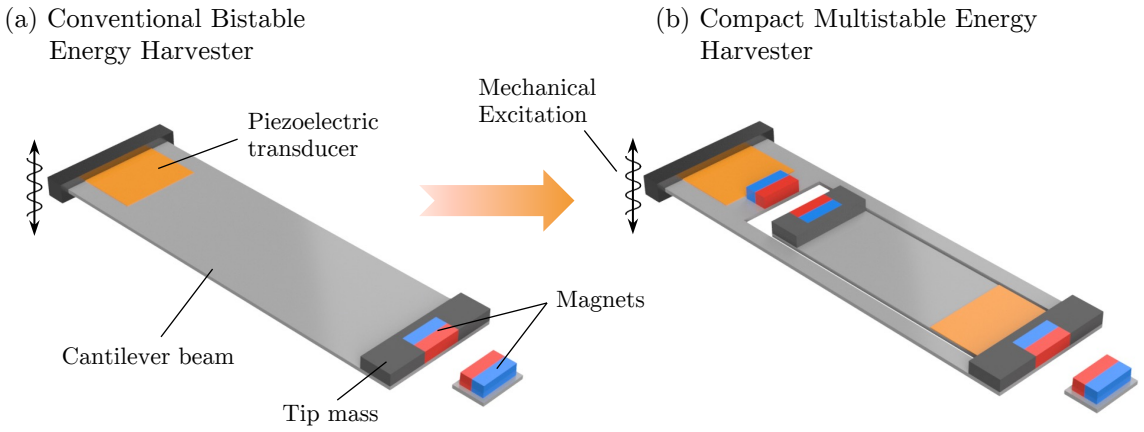

Figure 1 – Conceptual representation of the compact multistable energy harvester (CMEH), illustrating its compact and space-efficient design, which is comparable in size to the conventional bistable energy harvester (CBEH).

The CBEH and the CMEH can be represented by the dimensionless system of Equations 1 to 4. Equation 1 describes the motion of the outer beam, while Equation 2 describes the dynamics of the inner beam. Equations 3 and 4 are the expressions that represent the outer and inner piezoelectric elements, respectively.

$$\ddot{\bar{z}}_1 + 2\zeta_1\dot{\bar{z}}_1 - 2\zeta_2(\dot{\bar{z}}_2 - \dot{\bar{z}}_1) + (1+\alpha_1)\bar{z}_1 + \beta_1\bar{z}_1^3 - \rho\Omega_s^2(\bar{z}_2 - \bar{z}_1) - \chi_1\bar{v}_1 + \chi_2\bar{v}_2 = -\ddot{\bar{z}}_b; \tag{1}$$

$$\rho\ddot{\bar{z}}_2 + 2\zeta_2(\dot{\bar{z}}_2 - \dot{\bar{z}}_1) + \alpha_2\bar{z}_2 + \beta_2\bar{z}_2^3 + \rho\Omega_s^2(\bar{z}_2 - \bar{z}_1) - \chi_2\bar{v}_2 = -\ddot{\bar{z}}_b; \tag{2}$$

$$\dot{\bar{v}}_1 + \varphi_1\bar{v}_1 + \kappa_1\dot{\bar{z}}_1 = 0; \tag{3}$$

$$\dot{\bar{v}}_2 + \varphi_2\bar{v}_2 + \kappa_2(\dot{\bar{z}}_2 - \dot{\bar{z}}_1) = 0. \tag{4}$$

In this model, subscript $\square_1$ refers to the outer beam, while subscript $\square_2$ refers to the inner beam. The generalized coordinate $\bar{z}$ represents the relative displacement perpendicular to the larger surface of the beam, and $\bar{v}$ represents the voltage between the surfaces of each piezoelectric element. These generalized coordinates are functions of time, with $\bar{\square}$ denoting the time derivative. The mechanical dissipation coefficients are denoted by ζ. The polynomial coefficients α and β fit the total resulting nonlinear restitution force of the magnetic interactions. The ratio between the inner and outer equivalent masses is represented by ρ, and Ω_s is the ratio between the first natural frequencies of the inner and outer beams. The electromechanical couplings of the piezoelectric elements in the mechanical and electrical equations are denoted by χ and κ, respectively. The term φ is related to the inverse of the resistance in each piezoelectric equivalent circuit. Finally, $z_b = \gamma \sin(\Omega\tau)$ describes a harmonic support excitation, where γ is the amplitude, Ω is the frequency of excitation, and τ is time.

The conventional bistable harvester (CBEH) can be described by making $\rho = \Omega_s = \zeta_2 = \alpha_2 = \beta_2 = \chi_2 = \varphi_2 = \kappa_2 = 0$, while the CMEH is represented by all parameters different from zero. The performance of each harvester can be done by evaluating the total average output power of each harvester utilizing the following expressions:

$$\bar{P}_{\text{avg}}^{\text{CBEH}} = \varphi_1 \left(\bar{v}_1^{\text{RMS}}\right)^2, \tag{5}$$

$$\bar{P}_{\text{avg}}^{\text{CMEH}} = \sum_{i=1}^{2} \left[\varphi_i \left(\bar{v}_i^{\text{RMS}}\right)^2\right], \tag{6}$$

$$\tag{7}$$

where the superscript $\square^{\text{RMS}}$ refers to the root mean square (RMS) value of the generalized coordinate, defined as presented in Eq. 8. In this Equation, τ_0 and τ_f are the initial and final time of integration.

$$\square^{\text{RMS}} = \sqrt{\frac{1}{\tau_f - \tau_0} \int_{\tau_0}^{\tau_f} [\square(\tau)]^2 \, d\tau}, \tag{8}$$

The Multistable Hybrid Energy Harvester

The classical piezoelectric energy harvester (CPEH) consists of a cantilever beam with a piezoelectric transducer attached near the fixed end and a tip mass at the free end. The multidirectional hybrid energy harvester (MHEH) evolves from the CPEH by incorporating an additional pendulum at the free end, enabling multidirectional capabilities. Furthermore, an electromagnetic transducer is strategically placed at the pendulum's support to harness its rotational energy, thereby enhancing performance.

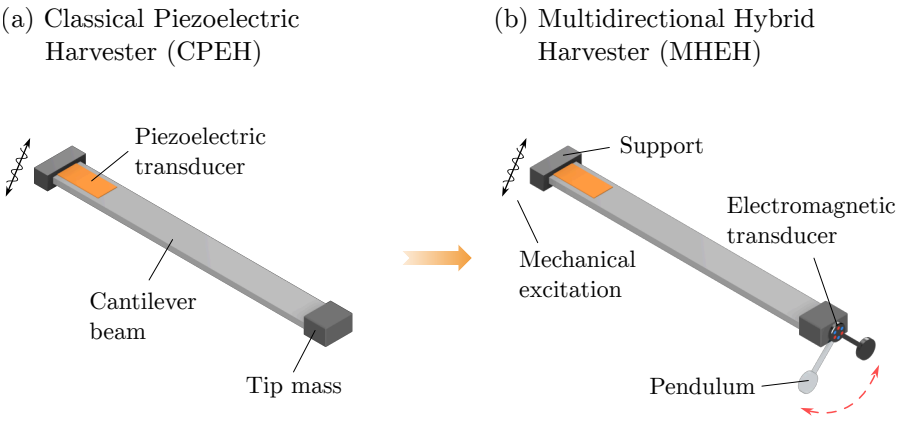

Figure 2 – Conceptual representation of the evolution of the classical piezoelectric energy harvester (CPEH) to the multidirectional hybrid energy harvester (HMEH). (a) The CPEH. (b) The HMEH.

The CPEH and the MHEH are described by the dimensionless system of Equations 9 to 13. Equations 9 and 10 depict the harvester's motion parallel and perpendicular to the wider surface of the beam, respectively. Equation 11 details the pendulum's dynamics, while Equations 12 and 13 describe the dynamics of the piezoelectric and electromagnetic transducers, respectively.

$$(1+\rho)\ddot{\bar{x}}+2\zeta_x\dot{\bar{x}}+\Omega_s^2\bar{x}+\rho\ell\left[\ddot{\bar{\phi}}\cos(\bar{\phi})-\dot{\bar{\phi}}^2\sin(\bar{\phi})\right]=-(1+\rho)\ddot{\bar{x}}_b; \tag{9}$$

$$(1+\rho)\ddot{\bar{z}}+2\zeta_z\dot{\bar{z}}+\bar{z}-\chi_{pz}\bar{v}-\rho\ell\left[\ddot{\bar{\phi}}\sin(\bar{\phi})+\dot{\bar{\phi}}^2\cos(\bar{\phi})\right]=-(1+\rho)\ddot{\bar{z}}_b; \tag{10}$$

$$\ddot{\bar{\phi}}+2\zeta_\phi\dot{\bar{\phi}}+\Omega_\phi^2\sin(\bar{\phi})-\chi_{em}\bar{I}+\frac{1}{\ell}\left[\ddot{\bar{x}}\cos(\bar{\phi})-\ddot{\bar{z}}\sin(\bar{\phi})\right]=\frac{1}{\ell}\left[\ddot{\bar{z}}_b\sin(\bar{\phi})-\ddot{\bar{x}}_b\cos(\bar{\phi})\right]; \tag{11}$$

$$\dot{\bar{v}}+\frac{\bar{v}}{\varphi_{pz}}+\kappa_{pz}\dot{\bar{z}}=0; \tag{12}$$

$$\dot{\bar{I}}+\varphi_{em}\bar{I}+\kappa_{em}\dot{\bar{\phi}}=0. \tag{13}$$

In this model, $\bar{x}$ and $\bar{z}$ are the generalized coordinates for the motions parallel and perpendicular to the larger surface of the beam, respectively, relative to the base support. Subscripts $\square_x$ and $\square_z$ indicate variables associated with the x and z directions. The generalized coordinate $\bar{\phi}$ corresponds to the angular position of the pendulum, with the subscript $\square_\phi$ referring to variables related to the pendulum. Variables with subscripts $\square_{pz}$ and $\square_{em}$ are associated with the piezoelectric and electromagnetic transducers, respectively. The generalized coordinates $\bar{v}$ and $\bar{I}$ represent the voltage in the piezoelectric circuit and the electrical current in the electromagnetic circuit, respectively. The constant ζ is associated with the system's dissipation coefficients. Ω_s is the ratio between the x and z natural frequencies, while Ω_ϕ is the ratio between the pendulum's natural frequency and that of the z direction. The dimensionless constant ℓ relates to the pendulum's length, and ρ is the ratio between the equivalent masses of the pendulum and the beam. The parameters χ and κ are associated with the electromechanical coefficients of the transducers, while φ relates to the equivalent resistances of each transducer circuit. The multidirectional support excitation is defined by the harmonic functions $\bar{x}_b=\gamma\sin(\Omega\tau)\sin(\bar{\mu})$ and $\bar{z}_b=\gamma\sin(\Omega\tau)\cos(\bar{\mu})$, where γ and Ω are the excitation amplitude and frequency, respectively, and $\bar{\mu}$ is the angle of the excitation with respect to the perpendicular direction of the larger beam surface.

The classical piezoelectric energy harvester (CPEH) can be described by making $\ell=\zeta_\phi=\Omega_\phi=\chi_{em}=\varphi_{em}=\kappa_{em}=0$, while the MHEH is represented by all parameters different from zero. The performance of each harvester is evaluated similarly to the previous harvesters, by computing the total average output power of each harvester using the following expressions:

$$\bar{P}_{\text{avg}}^{\text{CPEH}}=\frac{1}{\varphi_{pz}}\left(\bar{v}^{\text{RMS}}\right)^2, \tag{14}$$

$$\bar{P}_{\text{avg}}^{\text{MHEH}}=\frac{1}{\varphi_{pz}}\left(\bar{v}^{\text{RMS}}\right)^2+\varphi_{em}\left(\bar{I}^{\text{RMS}}\right)^2, \tag{15}$$

where the RMS values are also computed using Equation 8.

HARVESTERS' PERFORMANCE COMPARISON

In this section, a comparison between the CMEH and MHEH with their counterparts, CBEH and CPEH, is of concern. For each harvester, an Overall Performance Diagram (OPD) is presented, where the total average output power is computed for different points in a two-dimensional parameter space grid of $\gamma\times\Omega$. For each point, numerical integration is performed using the fourth-order Runge-Kutta method to obtain the solution of the nonlinear system of electromechanical equations, and the total average output power is computed. Then, a comprehensive performance comparison of the new harvesters with their counterparts is conducted. The CMEH is compared with the CBEH, and the MHEH is compared to the CPEH. The comparison is conducted using a Performance Comparison Diagram (PCD). Each point on their respective OPD is compared using a percentage difference metric, denoted as $\Delta\bar{P}(\%)$, as outlined in Equation 16. Here, P_r represents the performance metric of the reference harvester (the CBEH or the CPEH), while P_s denotes the performance metric of the harvester under study (the CMEH or the MHEH).

$$\Delta\bar{P}(\%)=\frac{P_s-P_r}{P_r}\times 100. \tag{16}$$

Equation 16 is used to compute the percentage difference, which allows a classification based on two sets:

- $\Delta\bar{P}(\%)\geq 0$: The harvester under study shows equal or better performance;

- $\Delta\bar{P}(\%) < 0$: The harvester used as reference shows better performance.

The simulation parameters utilized for all harvesters are displayed in Tab. 1.

Table 1 – Simulation parameters for the Harvesters.

CBEH vs CMEH

Parameter	CBEH Value	CMEH Value
Ω	$0.01 \rightarrow 10$	$0.01 \rightarrow 10$
γ	$0.01 \rightarrow 1$	$0.01 \rightarrow 1$
ρ	0	1
ζ_1	0.025	0.025
ζ_2	0	0.025
Ω_s	0	0.25
α_1	-2	-2
α_2	0	-1
β_1	1	1
β_2	0	1
χ_1	0.05	0.05
χ_2	0	0.05
κ_1	0.5	0.5
κ_2	0	0.5
φ_1	0.05	0.05
φ_2	0	0.05

CPEH vs MHEH

Parameter	CPEH Value	MHEH Value
Ω	$0.01 \rightarrow 2$	$0.01 \rightarrow 2$
γ	$0.01 \rightarrow 0.5$	$0.01 \rightarrow 0.5$
$\bar{\mu}$	45°	45°
ρ	0.5	0.5
ζ_x	0.025	0.025
ζ_z	0.025	0.025
ζ_ϕ	0	0.0025
Ω_s	1.87	1.87
Ω_ϕ	0	0.05
ℓ	0	1
χ_{pz}	0.05	0.05
χ_{em}	0	0.04
κ_{pz}	0.5	0.5
κ_{em}	0	0.4
φ_{pz}	1	1
φ_{em}	0	0.25

Figure 3 shows the results for the comparison between the CBEH and the CMEH. Figs 3a and 3b display the OPDs for the CBEH and the CMEH, respectively, where rainbow colors represent the magnitude of the total average output power of the harvesters. Purple colors represent low performance, while red colors represent high performance. The colors in between are considered medium performance. Both harvesters have very similar OPDs, with the same qualitative behavior, that is, low, medium, and high performance basically occur in the same region in the two-dimensional parameter space. Despite this similar characteristic, the CMEH displays almost double maximum performance when compared to the CBEH, as seen in the colorbars. A proper comparison is done by means of the PCD represented in Fig. 3c, where red colors represent where in the two-dimensional parameter space the CMEH outperforms the CBEH, while black regions show the opposite. The colorbar limits of the resulting PCD are truncated by 50% to better illustrate the difference between the two harvesters. In other words, the darker colors in each red or black colormap represent scenarios in which one harvester outperforms the other by a factor of 50% or more. Theoretically, the limit of the red percentage values is ∞, while the limit of the black percentage values is -100%, as the comparison is done utilizing the reference harvester (CBEH) as basis, as determined in Equation 16. By considering the regions of medium to high performance of both energy harvesters as the operational relevant scenarios, it is observed in the PCD in these regions that the CMEH outperforms the CBEH in almost all contexts.

Similarly, Fig. 4 shows the performance comparison of the CPEH and the HMEH. By analyzing the OPDs displayed in Figs. 4a and 4b, the narrow bandwidth of the CPEH is observed as previously described in the literature. The addition of the pendulum with the electromagnetic harvester drastically enhances the operational bandwidth of the device, however, the peak power is diminished, as displayed by the maximum magnitudes in the colorbars. Moreover, this reduction in maximum power in a small band is further evident in the PCD of Fig. 4c, showing that the only regions where the CPEH outperforms the HMEH is in the resonance regions of the CPEH and a small region next to it. In all other operational regions, the HMEH drastically outperforms the CPEH, as shown by the red colorbar truncated at 10000%.

Both CMEH and HMEH were designed with the proposed multi-harvesting strategy as the main paradigm. These results show that this paradigm, when utilized correctly, can drastically enhance the performance of the harvesters, almost maintaining the same size as the reference harvesters.

CONCLUSIONS

This work introduces a novel approach named ”multi-harvesting” to enhance the performance of energy harvesting devices. Multi-harvesting involves strategically integrating new transducers with multimodal capabilities, thereby intro-

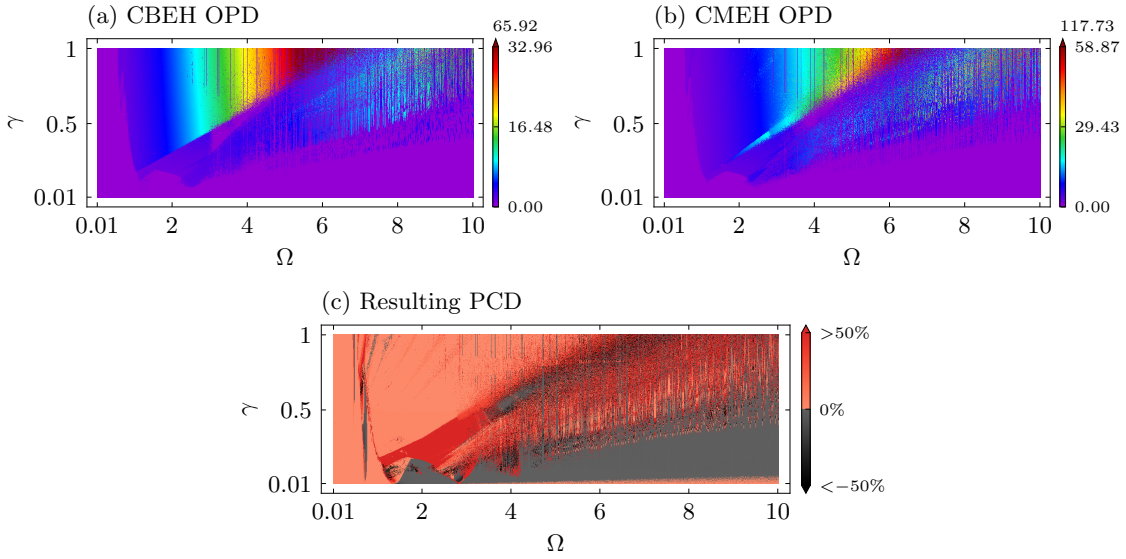

Figure 3 – Comparison between the CBEH and CMEH performances. (a) OPD for the CBEH, (b) OPD for the CMEH, (c) resulting PCD. Rainbow colors in (a) and (b) represent the total average output power of each harvester, and black and red colors in (c) represent the $\delta\bar{P}(\%)$ value, as represented in Equation 16.

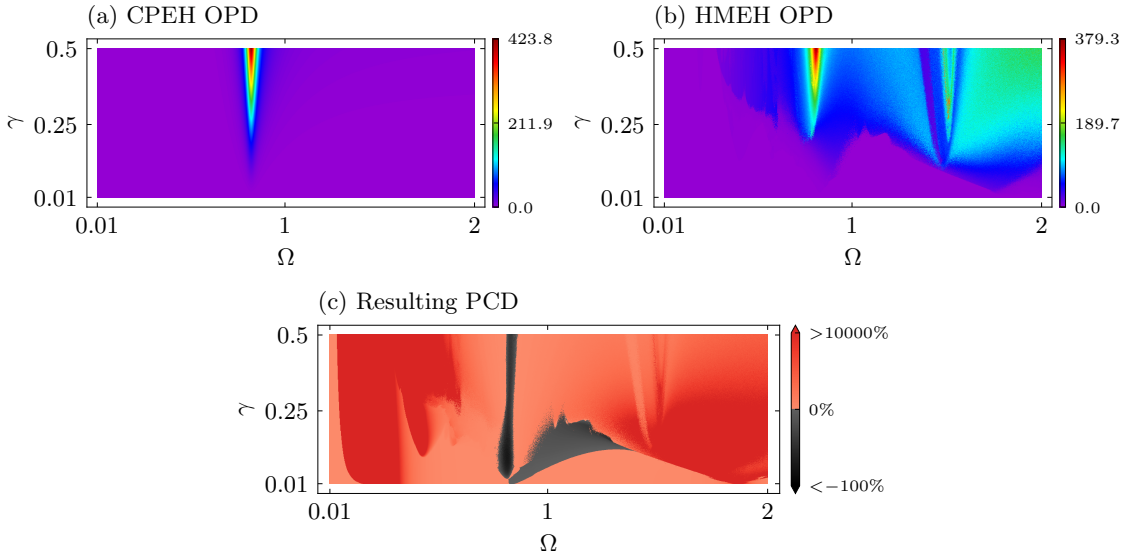

Figure 4 – Comparison between the CPEH and HMEH performances. (a) OPD for the CPEH, (b) OPD for the HMEH, (c) resulting PCD. Rainbow colors in (a) and (b) represent the total average output power of each harvester, and black and red colors in (c) represent the $\delta\bar{P}(\%)$ value, as represented in Equation 16.

ducing additional degrees of freedom to boost performance. To demonstrate this concept, two innovative designs are highlighted, derived from traditional models but optimized using the multi-harvesting strategy.

The first design evolves from the conventional bistable harvester by incorporating an inner beam with identical characteristics alongside the main beam. This adjustment utilizes previously unused space and introduces magnetic interactions, resulting in a compact, multistable harvester that maximizes efficiency.

The second design enhances the classical piezoelectric energy harvester by attaching a pendulum to the cantilever structure's free end. This modification enables multidirectional capabilities, while an additional electromagnetic transducer captures rotational energy from the pendulum's support.

Both designs are thoroughly modeled and compared against their traditional counterparts. Results demonstrate signif-

icant performance improvements achieved through the multi-harvesting paradigm while maintaining a comparable operational footprint. This underscores the potential of multi-harvesting as a transformative approach for designing compact and highly efficient energy harvesters.

REFERENCES

duToit, N. E., Wardle, B. L., Kim, S.-G. "Design considerations for MEMS-scale piezoelectric mechanical vibration energy harvesters", Integrated Ferroelectrics, v. 71, n. 1, pp. 121-160, 2005.

Faraday, M. "V. Experimental researches in electricity", Philosophical Transactions of the Royal Society of London, v. 122, pp. 125-162, 1832.

Liu, L., Guo, X., Liu, W., et al. "Recent progress in the energy harvesting technology - from self-powered sensors to self-sustained IoT, and new applications", Nanomaterials, v. 11, n. 11, 2021.

IEEE, 176-1987, A. S. "IEEE standard on piezoelectricity". 1987.

Apicella, V., Clemente, C. S., Davino, D., et al. "Review of modeling and control of magnetostrictive actuators", Actuators, v. 8, n. 2, 2019.

Erturk, A., Inman, D. J. "An experimentally validated bimorph cantilever model for piezoelectric energy harvesting from base excitations", Smart Materials and Structures, v. 18, n. 2, pp. 025009, 2009.

Costa, L. G., Monteiro, L. L. S., Pacheco, P. M. C. L., et al. "A parametric analysis of the nonlinear dynamics of bistable vibration-based piezoelectric energy harvesters", Journal of Intelligent Material Systems and Structures, v. 32, n. 7, pp. 699-723, 2021.

Ai, R., Monteiro, L. L. S., Monteiro, P. C. C., et al. "Piezoelectric vibration-based energy harvesting enhancement exploiting nonsmoothness", Actuators, v. 8, n. 1, 2019.

Zou, H.-X., Zhao, L.-C., Gao, Q.-H., et al. "Mechanical modulations for enhancing energy harvesting: Principles, methods and applications", Applied Energy, v. 255, pp. 113871, 2019.

Wu, H., Tang, L., Yang, Y., et al. "A novel two-degrees-of-freedom piezoelectric energy harvester", Journal of Intelligent Material Systems and Structures, v. 24, n. 3, pp. 357-368, 2013.

Costa, L. G., Savi, M. A. "Nonlinear dynamics of a compact and multistable mechanical energy harvester", International Journal of Mechanical Sciences, v. 262, pp. 108731, 2024.

Costa, L. G., Monteiro, L. L. S., Savi, M. A. "Multistability investigation for improved performance in a compact nonlinear energy harvester", Journal of the Brazilian Society of Mechanical Sciences and Engineering, v. 46, n. 4, pp. 212, 2024.

Costa, L. G., Savi, M. A. "Pendulum-based hybrid system for multidirectional energy harvesting". Nonlinear Dynamics, in review, 2024.

ACKNOWLEDGMENTS

The authors would like to acknowledge the support of the Brazilian Research Agencies CNPq (Conselho Nacional de Desenvolvimento Científico e Tecnológico), CAPES (Coordenação de Aperfeiçoamento de Pessoal de Nível Superior) and FAPERJ (Fundação Carlos Chagas Filho de Amparo à Pesquisa do Estado do Rio de Janeiro) and through the INCT-EIE (National Institute of Science and Technology - Smart Structures in Engineering), CNPq, CAPES and FAPEMIG (Fundação de Amparo à Pesquisa do Estado de Minas Gerais). The support of the AFOSR (Air Force Office of Scientific Research) is also acknowledged. Moreover, the authors also appreciate the use of the computational resources of the NACAD (Advanced High-Performance Computing Nucleus).

RESPONSIBILITY NOTICE

The authors are the only parties responsible for the printed material included in this paper.